How to cite: *Angew. Chem. Int. Ed.* **2023,** *62,* e202217372
International Edition: doi.org/10.1002/anie.202217372
German Edition: doi.org/10.1002/ange.202217372

Biocatalysis

Engineering a Highly Regioselective Fungal Peroxygenase for the Synthesis of Hydroxy Fatty Acids

*Patricia Gomez de Santos[+], Alejandro González-Benjumea[+], Angela Fernandez-Garcia[+], Carmen Aranda, Yinqi Wu, Andrada But, Patricia Molina-Espeja, Diana M. Maté, David Gonzalez-Perez, Wuyuan Zhang, Jan Kiebist, Katrin Scheibner, Martin Hofrichter, Katarzyna Świderek, Vicent Moliner, Julia Sanz-Aparicio, Frank Hollmann, Ana Gutiérrez, and Miguel Alcalde**

Abstract: The hydroxylation of fatty acids is an appealing reaction in synthetic chemistry, although the lack of selective catalysts hampers its industrial implementation. In this study, we have engineered a highly regioselective fungal peroxygenase for the ω-1 hydroxylation of fatty acids with quenched stepwise over-oxidation. One single mutation near the Phe catalytic tripod narrowed the heme cavity, promoting a dramatic shift toward subterminal hydroxylation with a drop in the over-oxidation activity. While crystallographic soaking experiments and molecular dynamic simulations shed light on this unique oxidation pattern, the selective biocatalyst was produced by *Pichia pastoris* at 0.4 g L^{-1} in a fed-batch bioreactor and used in the preparative synthesis of 1.4 g of (ω-1)-hydroxytetradecanoic acid with 95 % regioselectivity and 83 % *ee* for the *S* enantiomer.

Introduction

The selective synthesis of hydroxy fatty acids is of particular industrial interest, since these compounds can be used in a wide range of applications in the cosmetic, pharmaceutical and food industries, and for the production of resins, lubricants and biopolymers.[1–3] The selective hydroxylation of fatty acids at terminal and subterminal positions is of special note given the high C–H bond dissociation energies and the reliance on specific anchoring points for the carboxylate substrate moiety for regioselective hydroxylation.[4] These reactions are difficult to access by chemical means (i.e. using transition-metal catalysts) and therefore, for decades they have been studied with natural and/or engineered cytochrome P450 monooxygenases CYPs (EC 1.14.14.1), 12-hydroxylases (EC 1.14.14.139), α-dioxygenases (EC 1.13.111.92), lipoxygenases (EC 1.13.11.x) and hydratases (4.2.1.53). However, low production yields, a lack of selectivity and limited turnovers has meant these approaches have had limited success at the preparative scale.[5,6] Accordingly, the bulk synthesis of hydroxy fatty acids is mostly performed by whole cell fermentation, which is dependent on complex process engineering with high associated production costs.[7,8] In the past decade, fungal unspecific peroxygenases (UPOs, EC 1.11.2.1) have emerged

[*] P. Gomez de Santos[+]
Evoenzyme, S.L.
Parque Científico de Madrid, C/Faraday 7,
28049 Madrid (Spain)

A. González-Benjumea,[+] C. Aranda, Prof. A. Gutiérrez
Instituto de Recursos Naturales y Agrobiología
de Sevilla (IRNAS), CSIC
Av. Reina Mercedes 10, 41012 Seville (Spain)

A. Fernandez-Garcia,[+] Prof. J. Sanz-Aparicio
Department of Crystallography & Structural Biology,
Institute of Physical Chemistry "Rocasolano", CSIC
C/Serrano 119, 28006 Madrid (Spain)

Y. Wu, A. But, W. Zhang, Prof. F. Hollmann
Department of Biotechnology Institution,
Delft University of Technology
Van der Maasweg St, 9, 2629 HZ Delft (The Netherlands)

P. Molina-Espeja, D. M. Maté, D. Gonzalez-Perez, Prof. M. Alcalde
Department of Biocatalysis, Institute of Catalysis, CSIC
C/Marie Curie 2, 28049 Madrid (Spain)
E-mail: malcalde@icp.csic.es

J. Kiebist, Prof. K. Scheibner
Institute of Biotechnology Institution,
Brandenburg University of Technology Cottbus-Senftenberg
Universitätsplatz 1, 01968 Senftenberg (Germany)

Prof. M. Hofrichter
Department of Bio- and Environmental Sciences, TU Dresden,
International Institute Zittau
Markt 23, 02763 Zittau (Germany)

K. Świderek, Prof. V. Moliner
BioComp Group, Institute of Advanced Materials (INAM),
Universitat Jaume I
12071 Castellon (Spain)

[+] These authors contributed equally to this work.

as potential industrial biocatalysts as they have similar reactivity and substrate profiles as the well-studied CYPs, but without the need for auxiliary flavoproteins or expensive redox cofactors.[9] Regardless of their phylogenetic arrangement (i.e. the existence of short and long UPO protein families with different structural features and substrate preferences), all known UPOs to date are triggered simply by H_2O_2, which acts as the final electron acceptor and oxygen source, while they are extracellular, soluble and stable enzymes.[10] More significantly, the limits imposed by the oxidative uncoupling ("oxygen dilemma") of CYPs do not occur in UPOs, which can therefore provide thousands of turnovers in challenging sp^3-carbon (C–H) hydroxylation reactions.[11–13] However, despite their enormous potential in organic synthesis, the controlled regioselective hydroxylation of fatty acids by UPOs and related CYP peroxygenases has not yet been reported for two main reasons: i) the presence of stepwise over-oxidation of the hydroxy fatty acids produced, leading to the generation of keto fatty acid by-products; and ii) the absence of strict regioselectivity given that a range of positions can be hydroxylated, from ω to ω-n positions, or even the α and β positions.[5,6,14,15] Thus, while the synthesis of hydroxy fatty acids by UPOs has been investigated at the analytical level, their low regio- and chemoselectivity generally results in complex product mixtures of regio- and stereoisomers, as well as over-oxidation products. These phenomena have hampered the industrial implementation of this biotransformation, as has also been the case with CYPs.[6,16,17]

In recent years, we have subjected the long UPO from *Cyclocybe (Agrocybe) aegerita* (*Aae*UPO) to a series of directed evolution campaigns. These have ranged from efforts to improve its functional expression in yeasts, activity and stability in organic solvents, substrate promiscuity, and to adapt it to overcome hurdles in the production of agrochemicals and pharmaceuticals.[18] As generally observed with other long UPOs, the oxygenation of saturated fatty acids (C_{12}–C_{18}) by *Aae*UPO mostly produces a mixture of ω-1 and ω-2 hydroxy fatty acids in similar proportions, along with minor amounts of their keto derivatives.[19,20] In this study, we engineered an *Aae*UPO mutant for the selective hydroxylation of saturated fatty acids. This biocatalyst shows strict regioselectivity towards ω-1 hydroxylation and limited over-oxidation. This unique *Aae*UPO variant was overproduced in yeast, crystallized and characterized at both the biochemical and atomic levels. As a proof-of-concept of the potential of this highly selective biocatalyst, (ω-1)-hydroxytetradecanoic acid was synthesized on a preparative scale, opening a way for the industrial implementation of this biocatalytic process.

Results and Discussion

As a starting point for this study, we chose the *Aae*UPO secretion mutant obtained from an earlier directed evolution campaign for heterologous functional expression in *Saccharomyces cerevisiae* and *Pichia pastoris*.[21,22] To screen mutant libraries for the regioselective hydroxylation of saturated fatty acids, we prepared a high-throughput screening (HTS) assay based on the hydroxylation of 12-methoxydodecanoic acid (12-methoxylauric acid, MLA), which was synthesized chemically at high purity (Figures S1–S5, Table S1).[23] MLA served as a surrogate for tetradecanoic (myristic) acid as both compounds have significant structural similarities (Figure S1b). Hydroxylation at the ω-position of MLA produces a formaldehyde equivalent that can react with the Purpald reagent to generate a purple complex as readily followed at 550 nm with high sensitivity (Figure S6).[24] As such, this new MLA assay was validated to screen UPO mutant libraries, with a 5 μM limit of sensitivity to detect formaldehyde.

UPOs are considered hybrid enzymes that bring together oxygen transfer reactions (i.e. peroxygenase activity: two-electron oxidations fueled by H_2O_2, mimicking the peroxide shunt pathway of CYPs) with a peroxidase activity (one-electron oxidations, like classical peroxidases). To map the effect of mutations on the whole UPO reaction profile, the MLA screening assay was complemented with characteristic colorimetric HTS assays for peroxygenase and peroxidase activities (see the Supporting Information for details). We first carried out classical directed evolution based on random mutagenesis on the whole UPO gene. Unfortunately, we could not identify positive variants for ω-hydroxylation of MLA, and we concluded that the desired shift in regioselectivity would require performing structure-guided mutagenesis on the active site. To this end, the crystal structure of the *Aae*UPO secretion mutant resolved at a resolution of 1.2 Å was examined.[25] The three residues closest to the heme domain (Phe69, Phe121 and Phe199) form a tripod that acts as a platform for substrate positioning, while Phe76 and Phe191 regulate the entrance and exit of substrates to heme channel (Figure 1a). Interestingly, the side chains of Ala73, Ala77, Phe188, Thr192, and Ser241 seemed to have some implication for the configuration of the heme access channel. However, only the Ala77 residue located in the same plane as the Phe tripod (at a distance of ca. 4.4–5.0 Å from Phe121 and Phe69), pointed out towards the inner heme channel controlling the diameter of the heme channel (Figure 1b and c).

Therefore, any subtle modification at this position may affect substrate diffusion and its positioning for catalysis. Accordingly, Ala77 was subjected to saturation mutagenesis, and the corresponding mutant library was produced in *S. cerevisiae* and screened with MLA, along with a set of peroxygenase (nitrobenzodioxole (NBD), propranolol, naphthalene) and peroxidase (2,2′-azino-bis(3-ethylbenzothiazoline-6-sulfonic acid), ABTS) substrates. After three consecutive re-screenings, we found a clone (referred to as the Fett mutant) carrying the new A77L substitution that exhibited the strongest terminal hydroxylation response in the MLA assay (a 10-fold improvement over *Aae*UPO), with suppressed activity on NBD, propranolol and naphthalene, and half the parental activity towards ABTS. Hence, it would appear that narrowing the heme channel may be beneficial for the terminal hydroxylation of linear MLA, whereas it would seem to be detrimental for the conversion of sterically more demanding/bulkier aromatic substrates (see soaking complexes in Figure 3 and Figur-

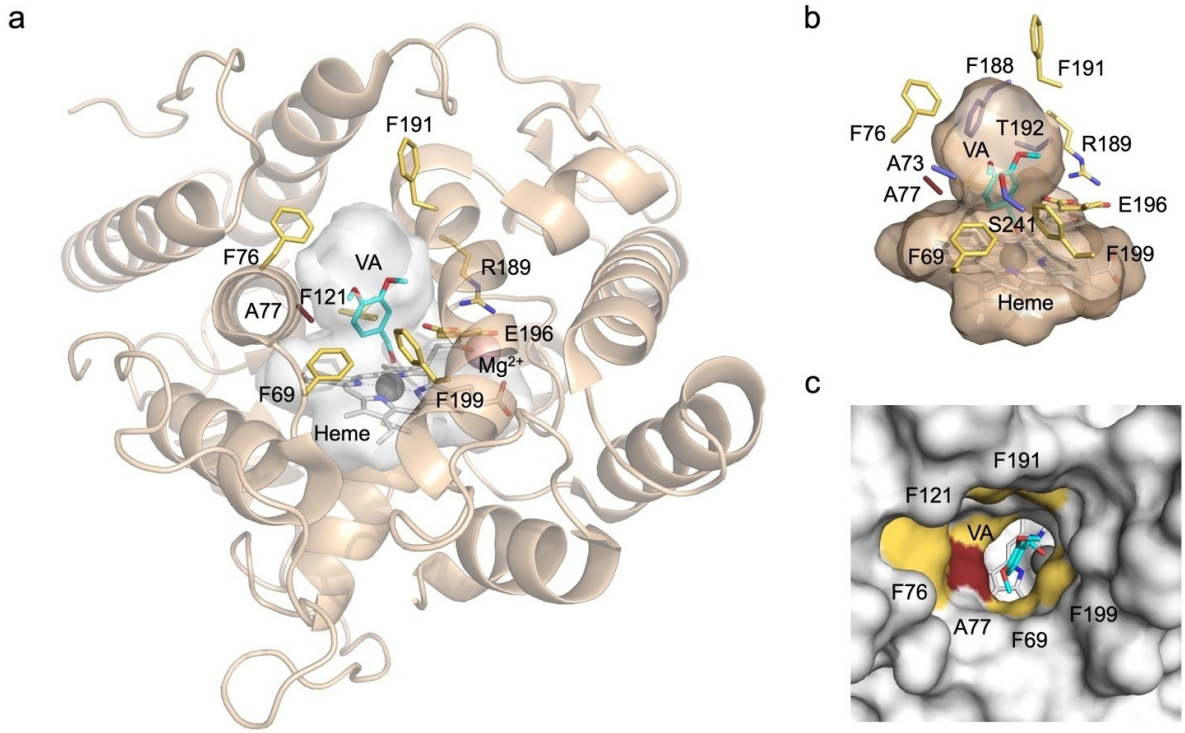

Figure 1. Rationale behind *Aae*UPO engineering. a) General view of the *Aae*UPO structure. The access and orientation of substrates is controlled by two apical Phe residues (Phe76 and Phe191, yellow sticks), and a Phe tripod located at the bottom of the heme channel (Phe69, Phe121, Phe191, yellow sticks). b) Potential residue candidates for mutagenesis configuring the shape of heme access channel (Ala73, Phe188, Thr192, and Ser241are shown as blue sticks and Ala77 in red sticks). Ala77 seems to exert a significant constriction in the shape of heme access channel determining substrate specificity. c) Upper view of the heme access channel in surface representation. The heme group is indicated as CPK colors, while the heme channel is highlighted in cavity mode. Veratryl alcohol (VA) is indicated in CPK color using cyan for carbon atoms. Acid-base pair Arg 189 and Glu 196 are colored in CPK using yellow for carbon atoms. PDB entry 6EL4.

es S15 and S16; see below). These observations were further confirmed when the initial turnover rates of the purified variants were measured with NBD, veratryl alcohol, benzyl alcohol, naphthalene (peroxygenase substrates) and ABTS (peroxidase substrate; Table 1).

The peroxygenase activity of the Fett mutant was hardly detected, while its peroxidase activity was somewhat limited. This is not surprising given that the substrates for oxygenation reactions must be placed in van der Waals distance from the deeply buried catalytic intermediate Compound I ($^{+\bullet}$Heme-Fe^{4+}=O). By contrast, the peroxidase activity of long UPOs is exclusively located at the entrance of the heme access channel, in good agreement with the retained activity observed for ABTS.[26]

Enzymatic reactions with *Aae*UPO and Fett were carried out using MLA as a substrate and their hydroxylating activity was assessed by gas chromatography-mass spectrometry (GC/MS). The only product observed in the Fett reaction was ω-hydroxylauric acid (Figure 2), reflecting strict regioselectivity for MLA terminal hydroxylation. No overoxidation was detected in this reaction (i.e. no aldehyde or carboxylate formation). By contrast, the parental *Aae*UPO

Table 1: Initial turnover rates (expressed as $\mu mol_{product}\,\mu mol_{UPO}^{-1}\,min^{-1}$) for peroxidase and peroxygenase substrates.

	*Aae*UPO		Fett mutant	
Substrate	Initial turnover rate	Activity [%][a]	Initial turnover rate	Activity [%][a]
ABTS	41275 ± 2747	100	17654 ± 1007	42.8
NBD	10065 ± 571	100	360 ± 28	3.6
veratryl alcohol	1806 ± 124	100	55 ± 2	3.0
benzyl alcohol	7571 ± 1784	100	342 ± 32	4.5
naphthalene	4917 ± 93	100	n.d.[b]	0

[a] Activity percentages were calculated by comparing *Aae*UPO and Fett mutant for each substrate tested. [b] Not detected.

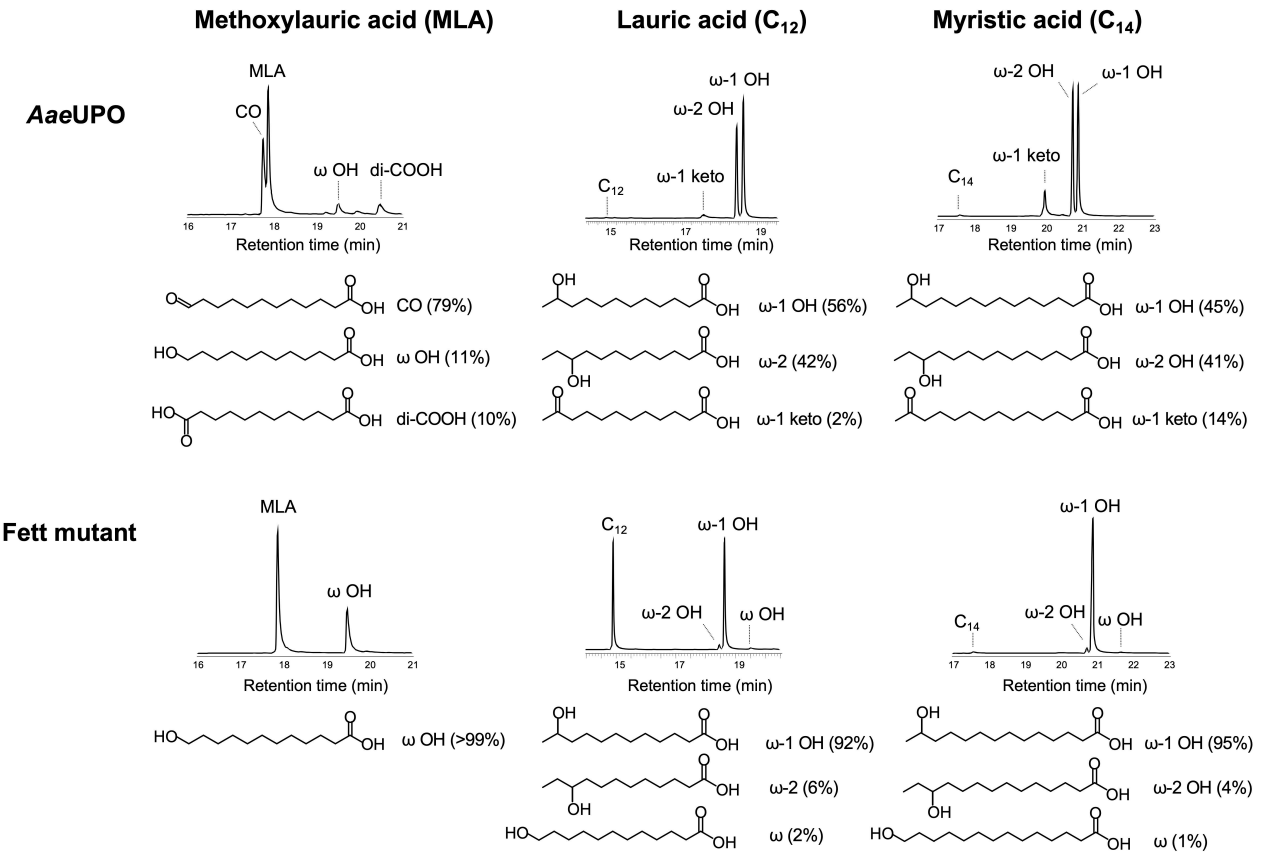

Figure 2. GC/MS analysis of the *Aae*UPO and Fett mutant reactions with methoxylauric acid (MLA), lauric acid (C12) and myristic acid (C14). Reactions were performed over 30 min at room temperature, and each reaction mixture contained 0.1 μM substrate, 2.5 mM H_2O_2, 0.1 μM purified enzyme and 20% (v/v) acetone in 100 mM potassium phosphate buffer pH 7.0.

yielded lauraldehyde (ω-oxolauric acid) as the main product (79%), reflecting the subterminal oxidation of MLA, along with minor amounts of ω-hydroxylauric acid (11%) and dodecanedioic acid (10%; Figure 2). Indeed, the latter might have been produced by the over-oxidation of lauraldehyde or ω-hydroxylauric acid. We analyzed this dramatic shift in regioselectivity and the drop in over-oxidation of the Fett mutant with a panel of saturated and unsaturated fatty acids, fatty acid methyl esters and alkanes: saturated lauric (C_{12}), myristic (C_{14}), palmitic (C_{16}) and stearic (C_{18}) acids, unsaturated palmitoleic ($C_{16:1}$) and oleic ($C_{18:1}$) acids, fatty acid methyl esters Me-C_{16}, Me-C_{18}, Me-$C_{16:1}$, Me-$C_{18:1}$ and the linear alkane tetradecane (Figure 2, Figures S7–S11, Table S2).

Although the chemical reactivity between MLA and fatty acids differs due to the presence of an ether group in MLA, the dramatic narrowing in regioselectivity observed for MLA was also evident when the mutant was assayed with saturated fatty acids. Fett converted lauric acid into (ω-1)-hydroxylauric acid (92%) with minor amounts of ω (2%) and ω-2 (6%) hydroxylated derivatives, again without showing stepwise over-oxidation of these products (Figure 2, Table S2). By contrast, *Aae*UPO transformed lauric acid into a mixture of ω-1 (56%) and ω-2 (42%) hydroxylated derivatives, together with minor amounts (2%) of (ω-1)-oxolauric acid as an over-oxidation product. This tightening in regioselectivity became even more evident when myristic acid was assessed, which has a similar size and shape to the surrogate MLA (Figure 2, Figure S1b, Table S2). With this substrate, Fett achieved almost complete conversion into (ω-1)-hydroxymyristic acid (95%) with minor amounts of ω (1%) and ω-2 (4%) hydroxylated derivatives and no over-oxidation products. Conversely, *Aae*UPO produced a mixture of ω-2 (41%) and ω-1 (45%) hydroxymyristic acids, along with 14% of (ω-1)-oxomyristic acid as over-oxidation by-product. Similar behavior was observed with palmitic and stearic acids, presenting even tighter regioselectivity towards ω-1 (Figure S7, Table S2). This particular combination of strict regioselective hydroxylation of the ω-1 subterminal position and reduced over-oxidation was also observed in the reactions of Fett with unsaturated palmitoleic and oleic fatty acids, as well as with the methyl esters of the above fatty acids and the alkane tetradecane (Figures S8–S11, Table S2).

We also evaluated the reactions of other positive clones found in the MLA mutant library (A77T and A77N), along with the *Aae*UPO mutants JaWa and SoLo, the latter identified in a previous directed evolution campaigns that

showed a promising reduction in the over-oxidation of aromatic compounds.[27,28]

In addition, we prepared a mutant that incorporated the A77L mutation into the SoLo variant (SoLo-A77L variant). Both *Aae*UPO mutants (JaWa and SoLo) converted myristic acid into a mixture of oxygenated (hydroxy and keto) derivatives at the ω-1 and ω-2 positions, with over-oxidized products predominating (Figure S12, Table S2). By contrast, A77T, A77N and SoLo-A77L showed relatively strict regioselectivity towards the ω-1 position, although only the former variant had relatively good myristic acid conversion and was able to transform lauric acid (and tetradecane) under the reaction conditions used. Though some of these designs increased the relative abundance of hydroxy fatty acids (particularly A77T), even at the ω-position, all in all they did not outperform the Fett variant in terms of balancing a defined selectivity with reduced over-oxidation and good substrate conversion.

To obtain sufficient Fett mutant for crystallization experiments and preparative scale-up reactions, it was cloned into *P. pastoris* and produced in a 12 L fed-batch bioreactor (Figure S13). We applied a strain screening method based on increasing concentrations of the antibiotic Zeocine, whereby we recovered a multicopy variant ($Fett_{pic}$) that yielded overproduction of 380 mg L^{-1} in bioreactor. To the best of our knowledge, this is the most efficient heterologous expression ever reported for a recombinant UPO.[29] $Fett_{pic}$ was purified to homogeneity (Figure S14), deglycosylated and analyzed in crystallography and soaking experiments with MLA, lauric acid, myristic acid, palmitoleic acid, *n*-tetradecane, *n*-hexane, naphthalene and ABTS. With the exception of ABTS, high-resolution crystal complexes (ranging from 2 to 1.5 Å) were obtained for all the substrates (Figure S15, Table S3).

The active site of UPO is a cone-shaped cavity that provides access to the heme group, with three Phe residues situated close together making up the base of the cone (Figure 1). These three Phe residues establish hydrophobic interactions with the substrates and are crucial to orientate them correctly for the reaction to occur, as witnessed in enzyme complexes with the peroxygenative substrate naphthalene, which binds at van der Waals distance from the heme (see soaking experiments in a cut-away mode, Figure S16a). However, in the $Fett_{pic}$ mutant, the Leu77 side chain protrudes into the heme channel and narrows the base of the cone so that there is only 3.6–4.4 Å between Leu77

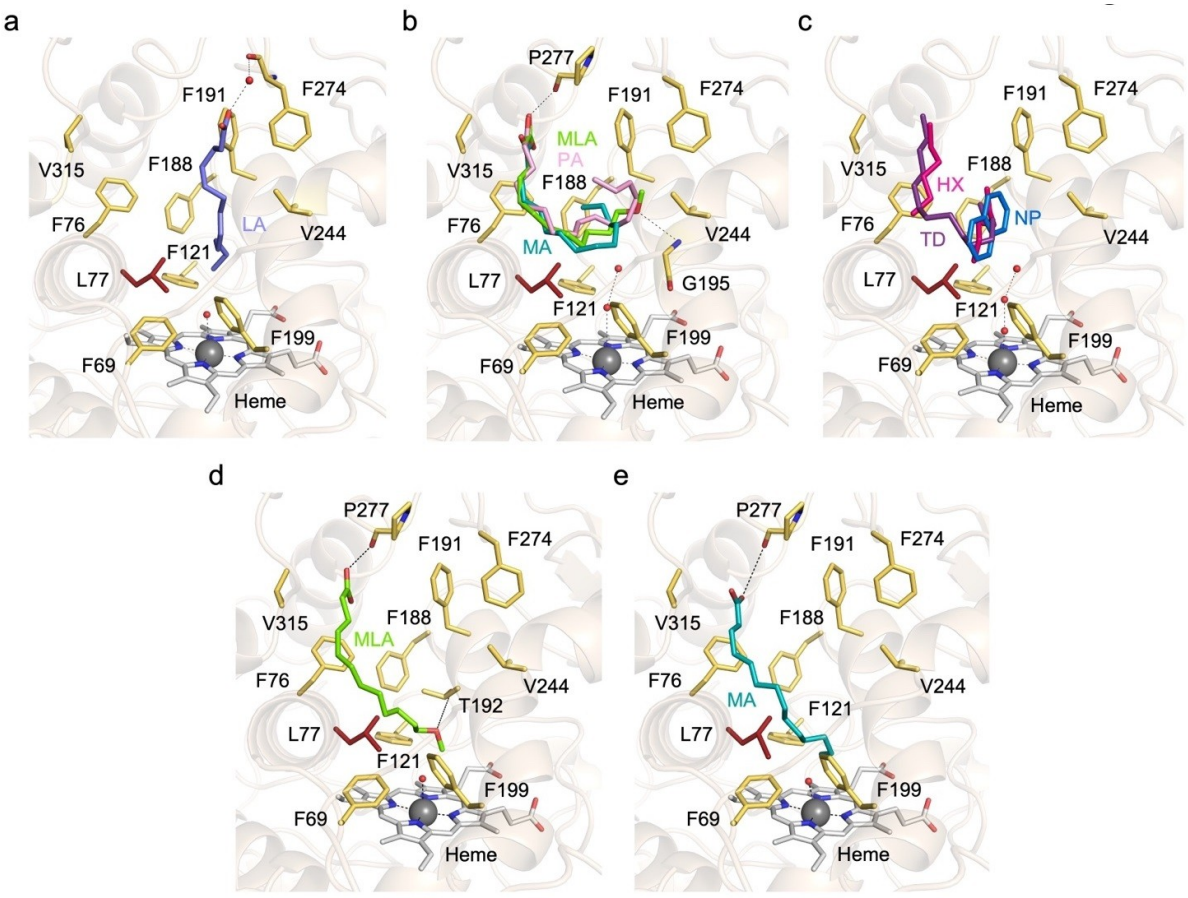

Figure 3. Crystallographic structure of the Fett complexes with a) lauric acid (LA), b) methoxylauric acid (MLA), myristic acid (MA) and palmitoleic acid (PA), and c) tetradecane (TD), hexane (HX) and naphthalene (NP). The relevant residues defining the heme channel are represented as sticks and polar bonds are shown as dashed lines. Water molecules involved in substrate recognition are included as red spheres. d), e) Proposed model of putative productive Fett complexes with MLA and MA.

and the three Phe residues that make up the tripod (Figure S16b). Indeed, this constricted funnel does not allow the entry of bulky substrates, explaining the severe decrease in peroxygenase activity described above against naphthalene, NBD, veratryl and benzyl alcohols (Table 1, Figures S15 and S16). Moreover, our soaking experiments revealed that lauric acid was the only substrate that approximates to the heme, and it was found at almost a van der Waals distance from the iron center, whereas most compounds evade the steric hindrance of the constriction that produces apparently unproductive complexes. However, these crystals are trapped in a conserved binding mode that reveals some relevant trends (Figure 3, Figure S15).

Two binding modes were observed for long-chain substrates, both defined mostly through interactions with the hydrophobic residues that conform the walls of the cavity, with only a few polar bonds. In the first binding mode, the carboxylate of the lauric acid is linked to the Phe274 main chain through a water molecule, while the distal C14 atom seems to be connected to the iron atom though an additional water molecule (Figure 3a). This last water molecule binds between the heme and the substrate, in a position similar to that reported for the distal oxygen of the ferric hydroperoxo intermediate. This organization would appear to mimic the first step of the reaction, representing a productive complex. Alternatively, in the second binding mode the carboxylates of MLA, myristic and palmitoleic acids are hydrogen-bonded to the Pro277 backbone (Figure 3b), with their aliphatic chain oriented mostly by stacking to Val 315 and Phe76. These hydrophobic interactions seem to be prevalent as the complexes with tetradecane and hexane show a similar positioning despite lacking the carboxylate polar link (Figure 3c). The remaining long chains of MLA, myristic and palmitoleic acids, and tetradecane, are arranged at the base of the cone similar to naphthalene and a second bound hexane molecule, all being at van der Waals distances of 4–5 Å from Leu77 and the Phe tripod. Only the oxygen atom from the terminal methoxy ether of MLA is also stabilized through a polar bond to the Gly195 backbone (Figure 3b).

Interestingly, highly dynamic substrate entry and passage along the UPO active site has been postulated due to trapping several molecules of propranolol or 1-naphthol in previous soaking experiments with the enzyme.[25] In fact, the position of naphthalene observed in the Fett$_{pic}$ variant is very close to that of the trapped 1-naphthol molecules in the UPO crystals. However, the further approximation of the bulky naphthalene towards the heme is prevented by Leu77 hindering the peroxygenation reaction. By contrast, the aliphatic chain of the other substrates may putatively overcome this constriction by situating their terminal reactive groups in a similar manner to that observed in the complex with lauric acid, a less stable state. Thus, by maintaining the same binding position as that observed, only a conformational rearrangement of their long chains would be necessary to situate the oxygen acceptor groups close to the iron, as illustrated by manual modelling of MLA (Figure 3d) and myristic acid (Figure 3e) in the Fett$_{pic}$ heme channel.

With the aim of having a more precise picture of the behavior of the Fett mutant, we performed computational studies through molecular dynamic simulations (MD). Harnessing the high-resolution crystal structures, 0.5 μs MD for *Aae*UPO and Fett variants with myristic acid (MA) as a substrate and the reactive oxo ferryl cation radical complex ($^{+\bullet}$Heme-Fe^{4+}=O), Compound I, as a cofactor, were carried out. Analysis of the results demonstrated that in the parental enzyme both C13 and C12 access Fe=O oxygen with similar frequencies, and therefore we can predict that the probability of abstracting a hydrogen atom from both carbon atoms by oxygen must be comparable (Figure 4a). This situation changes, however, in the Fett variant. In this case, it is C13 that mostly occupies the closest position to the Fe=O group (Figure 4a). These results are consistent with the rather poor regioselectivity of *Aae*UPO and the almost exclusive ω-1 selectivity of Fett. As shown in Figure 4b, the substrate is much more flexible in the *Aae*UPO than the Fett variant, adopting bent conformations. In contrast, in the Fett variant, the substrate is stretched out with the limited possibility of movement, which is dictated by the presence of Leu in its proximity (see movie in the Supporting Information). To explain the lack of over-oxidation of the resulting product (ω-1)-hydroxymyristic acid (ω-1-OH-MA) in the Fett mutant, we performed additional 1.0 μs MD simulations with ω-1-OH-MA as a substrate and Compound I as cofactor. The results confirmed a different behaviour of ω-1-OH-MA in the active site as compared to the original substrate, MA. In this case, two different conformers are observed, that is, reactive and non-reactive in both variants (Figure 4c) as defined by the distance between the Fe=O group and the hydrogen atom that can be abstracted in the first step of the over-oxidation process (Figure 4d). The presence of two conformers can explain why there is only partial formation of the oxidation product in *Aae*UPO, and why ω-1-OH-MA is not completely utilized in this process. However, the possibility of the competitive binding of alternative substrates that contribute to the experimental observations cannot be excluded. In the case of the Fett variant, the reactive conformer is also observed along simulations. However, it is less populated than the non-reactive conformer: 1.1 % reactive vs. 3.0 % non-reactive, in contrast to *Aae*UPO, where the opposite trend is observed: 2.5 % reactive vs. 2.2 % non-reactive.

The preparative synthesis of (ω-1)-hydroxymyristic acid was used to showcase the synthetic potential of the Fett$_{pic}$ mutant, an important bio-based building block for the production of polyester homopolymers. For preparative applications, the H_2O_2 concentration must be controlled to minimize the undesired oxidative inactivation of the biocatalyst.[30] In contrast to the parental *Aae*UPO, Fett$_{pic}$ showed almost no activity with the milder oxidant tert-butyl hydroperoxide (Figure S18a), possibly because the steric demands of the tert-butyl group hindered interactions with the catalytic heme site of Fett$_{pic}$. Therefore, we decided to use a H_2O_2-fed batch strategy in which H_2O_2 was added continuously. To increase the solubility of the hydrophobic starting material we evaluated different water miscible co-solvents, since the aqueous solubility of myristic acid at

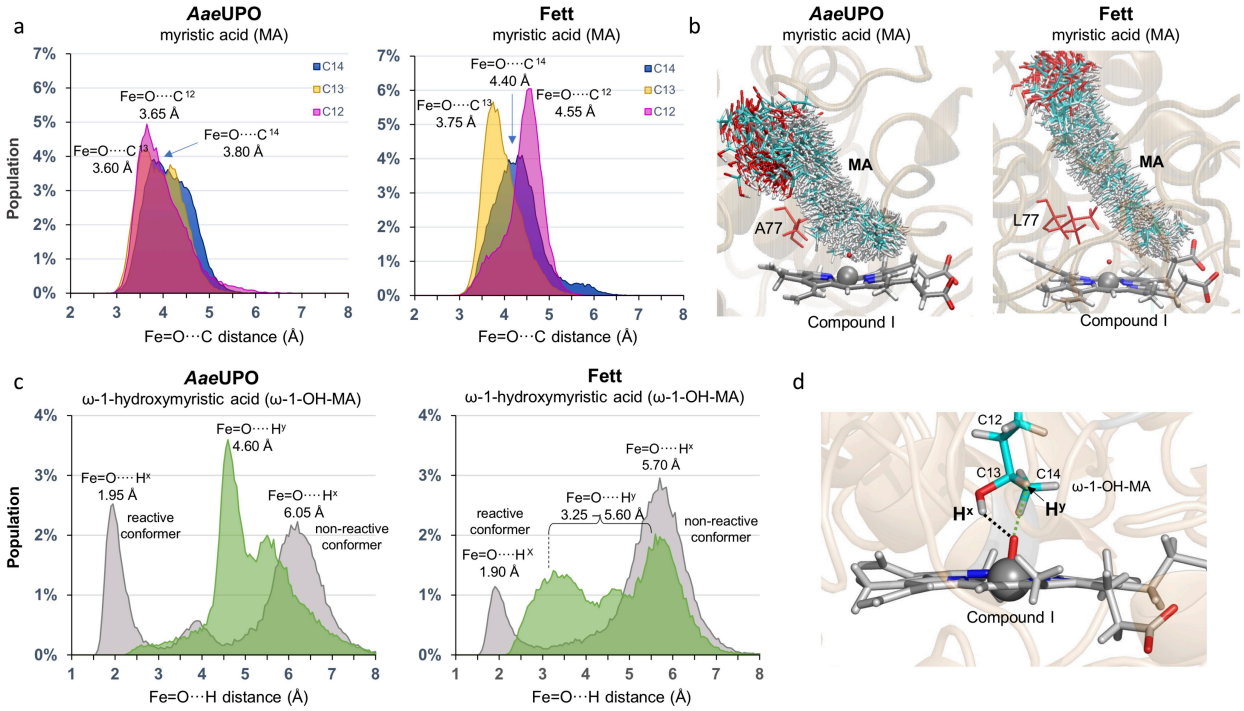

Figure 4. Geometrical analysis derived from MD simulations for the *Aae*UPO and Fett variants with the reactive oxo ferryl cation radical complex ($^{+\bullet}$Heme-Fe^{4+}=O), Compound I, as a cofactor and the myristic acid (MA) and (ω-1)-hydroxymyristic acid (ω-1-OH-MA) as substrates. a) Population analysis of key distances in the first step of the oxidation process with MA as a substrate, based on 40 000 snapshots. b) Overlay of MA conformers adopted along MD simulations in *Aae*UPO and Fett variants. c) Population analysis of key distances in the first step of the over-oxidation process with ω-1-OH-MA as a substrate, based on 100 000 snapshots. d) Detail of the active site with key atoms labelled. See also Figure S17 and Tables S4–S7.

20 °C is 55 mg L^{-1} (corresponding to 0.24 mM). Of the co-solvents investigated (acetone, methanol, isopropanol and tert-butanol; Figure S18b), acetone produced the best results, with negligible product formation in the presence of isopropanol or methanol. Product formation in the presence of tert-butanol was mildly impaired relative to acetone, albeit not as severely as with isopropanol or methanol. The poor performance of these primary/secondary alcohols may be explained by their direct oxidation by Fett$_{pic}$.

In a first set of experiments, we used 60 % (v/v) acetone as cosolvent in 50 mM phosphate buffer pH 7.0 containing 50 mM myristic acid and 25 μM Fett. The reaction was triggered with H_2O_2 supplied with a syringe pump for 50 min of a total reaction time of 1 h. The product mixture was analyzed by GC/MS, yielding 83 % conversion and 96 % of (ω-1)-hydroxymyristic acid. Despite the apparent suitability of acetone, we decided to replace it with tert-butanol in order to avoid the possible formation of explosive acetone peroxides; we also reduced the concentration of biocatalysts —up to 1.2 μM—to attain more economical reaction conditions. Two independent batch conversions on a litre scale (using 50 mM or 100 mM myristic acid: SC-1 and SC-2, Table S8) were performed using a very conservative H_2O_2 feeding strategy (1 mM h^{-1}). Interestingly, under these conditions, some over-oxidation of the primary hydroxylation product to the corresponding ketone was observed. Overall, approximately 30 % over-oxidation product was detected. Most likely, this can be attributed to the very long reaction times (4–7 days) giving the biocatalyst sufficient time to also convert the kinetically unfavoured hydroxyl product. Purification of the desired (ω-1)-hydroxymyristic acid was straightforward by flash chromatography, yielding gram amounts (up to 1.4 g) of essentially pure (ω-1)-hydroxymyristic acid (Table 2).

Both the selectivity of the enzymatic conversions and the purity of the final purified product were confirmed by ^{1}H NMR spectroscopy (Figures S19 and S20). All CYPs and UPOs described to date show a lack of regioselectivity and generate over-oxidation products. As such, they can only transform myristic acid into a mixture of hydroxy fatty acids that range from ω-1 to ω-9 (depending on the enzyme variant) and that produce keto by-products from very low substrate loadings (0.5 to 1 mM in the best of all cases).[5] Our system can function with up to 100 mM substrate loading and depending on the amount of enzyme used, respectable total turnovers of 4800 and approximately 15 000 were attained.

Finally, we determined the enantioselectivity of the reaction using the Mosher method based on comparisons of ^{1}H, ^{13}C and ^{19}F NMR spectra (Figures S21–S23) from the

Table 2: Scale-up experiments for the synthesis of (ω-1)-hydroxymyristic acid.[a]

	SCU-1	SCU-2
$[\text{Myristic acid}]_{initial}$ [mM][b]	48.4	28.5
$[(\omega\text{-}1)\text{-OH-myristic acid}]_{final}$ [mM]	18.4	19.3
$[(\omega\text{-}1)\text{-keto-myristic acid}]_{final}$ [mM]	6.8	5.1
Isolated yield/purity [g]/[%][c]	1.4/ > 90	1.2

[a] The reactions were initiated by starting a continuous feed of H_2O_2 (1 mM/h from a 100 mM stock solution). The reactions were terminated after 164 h by acidification of the reaction mixture to approximately pH 3.1. The crude product mixture was filtrated, washed with warm MTBE and purified by flash chromatography using petrol ether (40/60) : MTBE (3 : 1). [b] Calculated based on the final volume of the reaction mixture, real initial concentrations were approximately two times higher. [c] Isolated yield of purified (ω-1)-hydroxymyristic acid. After column chromatography, other fractions with lower purity were obtained (SCU-1: 3.1 g, SCU-2: 0.7 g), which were not included in the yield calculation of the isolated product. See also Table S8.

pair of α-methoxy-α-trifluoromethylphenylacetic acid (MTPA)-hydroxymyristic acid diastereomers (*X*,*S*) and (*X*,*R*). They were obtained from the methylated hydroxy acid by acylation with the corresponding enantiomerically pure Mosher acid chloride (MTPA-Cl) in the presence of 4-(dimethylamino)pyridine (DMAP; Scheme 1).

In all cases, two sets of signals were obtained from the recorded spectra, showing a pair of enantiomers produced by Fett. These distinguishable families of signals are related to the environment of the carbon stereocenter (C13 of methyl 13-hydroxymyristate) in ^{1}H and ^{13}C NMR spectra and the trifluoromethyl group (Mosher acid) in ^{19}F NMR spectra, so the following discussion refers to the main enantiomer observed. H14 protons (1.25 and 1.33 ppm) showed a strong shielding effect in ^{1}H NMR spectroscopy (−40 Hz using the $\delta(X,S)$-$\delta(X,R)$ convention), and the signals are shifted upfield when (*X*,*S*) is considered owing to the anisotropic effect caused by the aromatic ring. This result correlates to an ipsilateral position of H14 protons to the phenyl group, giving an *S* configuration. The ^{13}C spectra were in agreement with the above because the C14 (19.6 and 20.0 ppm) experienced an anisotropic shift upfield (−50 Hz) considering the (*X*,*S*) diastereomer. In addition, chemical shifts of the trifluoromethyl groups of each diastereomer (−71.49 and −71.44 ppm) also contributed to the assignment of the absolute configuration. In this case, the trifluoromethyl group of the (*X*,*S*) diastereomer was shifted downfield, which is compatible with an ipsilateral position of the larger group of the Mosher moiety (aromatic ring) to the smaller group of the hydroxy acid moiety (C14) giving an *S* configuration of the main enantiomer in agreement with the ^{1}H and ^{13}C spectra. Finally, according to ^{19}F NMR integrals, we determined a value of 83.4 % *ee* in favor of the *S* enantiomer.

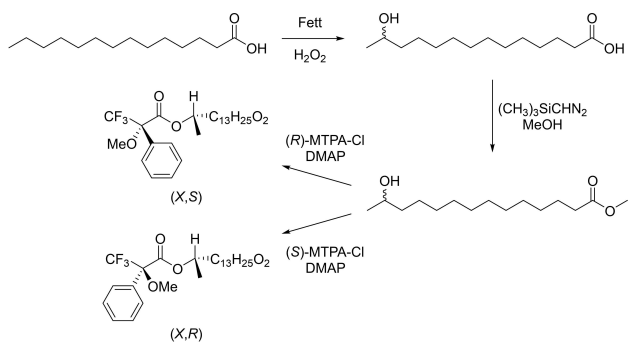

Scheme 1. Synthesis of methyl MTPA-13-hydroxymyristate from myristic acid. Structures of (*X*,*S*) and (*X*,*R*) diastereomers from the main enantiomer ((*S*)-hydroxymyristic acid) are included.

Despite the high regioselectivity of the Fett mutant, admittedly, our study provides only a proof-of-concept for its preparative applicability, and further improvements will be necessary to obtain economically feasible reaction schemes. Particularly the significant volume increase due to the external addition of H_2O_2 needs further attention. At the end of the reactions, the total volume had approximately doubled. In situ provision of H_2O_2 through catalytic O_2 reduction[30] will eliminate the volume increase issue and further contribute to the establishment of more robust processes. Another limitation of the current system lies in the over-oxidation of the desired hydroxy fatty acid to the corresponding keto acid when working at high substrate loads. The main reason for this observation lies in the high conversion of the original starting material and accumulation of the hydroxy product as a potential Fett substrate. We will address this issue in future studies by making use of the so-called two liquid phase system approach, in which a hydrophobic organic phase will serve as substrate reservoir (enabling higher reagent payloads) and product sink (thereby removing the hydroxylated product from the aqueous reaction layer and protecting it from further oxidation). Overall, we are convinced that the Fett mutant exhibits enormous potential as a biocatalyst for the large-scale preparation of hydroxy fatty acids.[5]

Conclusion

Exclusive hydroxylation at terminal and subterminal positions of fatty acids and linear alkanes requires specific control of the orientation of the side chain, while not causing over-oxidation of the released products. If this were not the case, a range of positions would be hydroxylated, and further over-oxidized to oxo and carboxylate by-products. Although considerable engineering efforts have been made over the years, a biocatalyst that brings these two characteristics together still has yet to be reported. In this study, one precise substitution at the inner heme channel of an evolved

peroxygenase was responsible for such a dramatic change, focusing regioselectivity exclusively at ω-1 while reducing unwanted over-oxidation. This biocatalyst proved to be effective in the bulk synthesis of ω-1 hydroxy fatty acids, making it the first of its kind to combine strict regioselective control with reduced over-oxidation, and opening the way for future applications. Indeed, this mutant can be over-produced by yeast in fed-batch fermentation, and with some further reaction engineering effort, the biocatalytic process presented herein could be readily scaled up for the production of desired ω-1 hydroxy fatty acids to be used as building blocks in the synthesis of valuable biopolymers and chemicals.

Acknowledgements

This work was supported by the European Union Project grant H2020-BBI-PPP-2015-2-720297-ENZOX2; the Spanish projects PID2019-106166RB-100-OXYWAVE, PID2020-118968RB-100-LILI, PID2021-123332OB-C21 and PID2019-107098RJ-I00, funded by the Ministerio de Ciencia e Innovación/Agencia Estatal de Investigación (AEI)/doi: 10.13039/501100011033/; the "Comunidad de Madrid" Synergy CAM project Y2018/BIO-4738-EVOCHIMERA-CM; the Generalitat Valenciana projects CIPROM/2021/079-PROMETEO and SEJI/2020/007; and the PIE-CSIC projects PIE-202040E185 and PIE-201580E042. P.G.d.S. thanks the Ministry of Science, Innovation and Universities (Spain) for her FPI scholarship (BES-2017-080040) and the Ministry of Science and Innovation for her contract as part of the PTQ2020-011037 project funded by MCIN/AEI/10.13039/501100011033 within the NextGenerationEU/PRTR. D.G.-P. thanks Juan de la Cierva Incorporación contract Ref. No.: IJC2020-043725-I, funded by MCIN/AEI/10.13039/501100011033, and the EU NextGenerationEU/PRTR program. K.Ś. thanks to Ministerio de Ciencia e Innovación and Fondo Social Europeo for a Ramón y Cajal contract (Ref. RYC2020-030596-I). We thank the Synchrotron Radiation Source at Alba (Barcelona, Spain) for assistance with the BL13-XALOC beamline.

Conflict of Interest

The authors declare no conflict of interest.

Data Availability Statement

Research data are not shared.

Keywords: Hydroxy Fatty Acids · Over-Oxidation · Protein Engineering · Regioselectivity · Unspecific Peroxygenase

[1] J. O. Metzger, U. Bornscheuer, *Appl. Microbiol. Biotechnol.* **2006**, *71*, 13–22.
[2] H. Mutlu, M. A. R. Meier, *Eur. J. Lipid Sci. Technol.* **2010**, *112*, 10–30.
[3] Y.-C. Joo, D.-K. Oh, *Biotechnol. Adv.* **2012**, *30*, 1524–1532.
[4] J. B. Johnston, H. Ouellet, L. M. Podust, P. R. Ortiz de Montellano, *Arch. Biochem. Biophys.* **2011**, *507*, 86–94.
[5] L. Hammerer, C. K. Winkler, W. Kroutil, *Catal. Lett.* **2018**, *148*, 787–812.
[6] C. Aranda, J. Carro, A. González-Benjumea, E. D. Babot, A. Olmedo, D. Linde, A. T. Martínez, A. Gutiérrez, *Biotechnol. Adv.* **2021**, *51*, 107703.
[7] K.-R. Kim, D.-K. Oh, *Biotechnol. Adv.* **2013**, *31*, 1473–1485.
[8] A.-Q. Yu, N. K. Pratomo Juwono, S. S. J. Leong, M. W. Chang, *Front. Bioeng. Biotechnol.* **2014**, *2* (78), 1–12.
[9] M. Hofrichter, R. Ullrich, *Curr. Opin. Chem. Biol.* **2014**, *19*, 116–125.
[10] M. Hofrichter, H. Kellner, R. Herzog, A. Karich, J. Kiebist, K. Scheibner, R. Ullrich, *Antioxidants* **2022**, *11*, 163.
[11] D. Holtmann, F. Hollmann, *ChemBioChem* **2016**, *17*, 1391–1398.
[12] M. Hobisch, D. Holtmann, P. Gomez de Santos, M. Alcalde, F. Hollmann, S. Kara, *Biotechnol. Adv.* **2021**, *51*, 107615.
[13] J. Münch, P. Püllmann, W. Zhang, M. J. Weissenborn, *ACS Catal.* **2021**, *11*, 9168–9203.
[14] A. Olmedo, J. C. del Río, J. Kiebist, R. Ullrich, M. Hofrichter, K. Scheibner, A. T. Martínez, A. Gutiérrez, *Chem. Eur. J.* **2017**, *23*, 16985–16989.
[15] A. W. Munro, K. J. McLean, J. L. Grant, T. M. Makris, *Biochem. Soc. Trans.* **2018**, *46*, 183–196.
[16] M.-C. Sigmund, G. J. Poelarends, *Nat. Catal.* **2020**, *3*, 690–702.
[17] G. Grogan, *JACS Au* **2021**, *1*, 1312–1329.
[18] A. Beltrán-Nogal, I. Sánchez-Moreno, D. Méndez-Sánchez, P. Gómez de Santos, F. Hollmann, M. Alcalde, *Curr. Opin. Struct. Biol.* **2022**, *73*, 102342.
[19] A. Gutiérrez, E. D. Babot, R. Ullrich, M. Hofrichter, A. T. Martínez, J. C. del Río, *Arch. Biochem. Biophys.* **2011**, *514*, 33–43.
[20] E. D. Babot, J. C. del Río, L. Kalum, A. T. Martínez, A. Gutiérrez, *Biotechnol. Bioeng.* **2013**, *110*, 2323–2332.
[21] P. Molina-Espeja, E. Garcia-Ruiz, D. Gonzalez-Perez, R. Ullrich, M. Hofrichter, M. Alcalde, *Appl. Environ. Microbiol.* **2014**, *80*, 3496–3507.
[22] P. Molina-Espeja, S. Ma, D. M. Mate, R. Ludwig, M. Alcalde, *Enzyme Microb. Technol.* **2015**, *73–74*, 29–33.
[23] A. Faig, L. K. Petersen, P. V. Moghe, K. E. Uhrich, *Biomacromolecules* **2014**, *15*, 3328–3337.
[24] P. Meinhold, M. W. Peters, A. Hartwick, A. R. Hernandez, F. H. Arnold, *Adv. Synth. Catal.* **2006**, *348*, 763–772.
[25] M. Ramirez-Escudero, P. Molina-Espeja, P. Gomez de Santos, M. Hofrichter, J. Sanz-Aparicio, M. Alcalde, *ACS Chem. Biol.* **2018**, *13*, 3259–3268.
[26] P. Molina-Espeja, A. Beltran-Nogal, M. A. Alfuzzi, V. Guallar, M. Alcalde, *Front. Bioeng. Biotechnol.* **2021**, *9*, 741282.
[27] P. Molina-Espeja, M. Cañellas, F. J. Plou, M. Hofrichter, F. Lucas, V. Guallar, M. Alcalde, *ChemBioChem* **2016**, *17*, 341–349.
[28] P. Gomez de Santos, M. Cañellas, F. Tieves, S. H. H. Younes, P. Molina-Espeja, M. Hofrichter, F. Hollmann, V. Guallar, M. Alcalde, *ACS Catal.* **2018**, *8*, 4789–4799.
[29] A. Kinner, K. Rosenthal, S. Lütz, *Front. Bioeng. Biotechnol.* **2021**, *9*, 705630.
[30] B. O. Burek, S. Bormann, F. Hollmann, J. Z. Bloh, D. Holtmann, *Green Chem.* **2019**, *21*, 3232–3249.

Manuscript received: November 28, 2022
Accepted manuscript online: December 30, 2022
Version of record online: January 24, 2023